Vietnam Journal of Catalysis and Adsorption
Tạp chí xúc tác và hấp phụ Việt Nam

http://chemeng.hust.edu.vn/jca/

Synthesis of WO_3/Ag_3VO_4 photocatalyst with enhanced visible light efficiency photocatalysis

Nguyen Thi Phuong Le Chi[1*], Tran Thi Thu Phuong[2], Do Minh The[2], Nguyen Tri Quoc[3], Nguyen Thi Thanh Binh[2], Tran Thi Thu Hien[2], Mai Hung Thanh Tung[4], Nguyen Vu Ngoc Mai[2], Phan Thi Dieu[2], Nguyen Thi Dieu Cam[2]

[1]*Hochiminh City University of Natural Resources and Environment, 236B Le Van Sy Street, Ward 1, Tan Binh District, Hochiminh City, Vietnam*
[2] *Faculty of Natural Sciences, Quy Nhon University, 170 An Duong Vuong, Quy Nhon City, Binh Dinh, Viet Nam*
[3] *Mien Trung industry and trade college, Viet Nam, 261 Nguyen Tat Thanh, Tuy Hoa City, Phu Yen, Viet Nam*
[4]*Chemical Engineering, Ho Chi Minh City University of Food Industry, 140 Le Trong Tan, Ho Chi Minh City, Viet Nam*
**Email: ntplchi@hcmunre.edu.vn*

ARTICLE INFO

Received: 10/5/2022
Accepted: 10/7/2022
Published: 15/7/2022

Keywords:

WO_3/Ag_3VO_4, photocatalyst; degradation, Amoxicillin, antibiotic pollutant, visible region

ABSTRACT

WO_3/Ag_3VO_4 photocatalyst was synthesized for benefiting the visible region of solar spectrum for degradation of antibiotic pollutant. The prepared catalyst was characterized by using scanning electron microscope (SEM), X-ray diffraction (XRD), infrared spectroscopy (IR) and energy-dispersive X-ray spectroscopy (EDX). The photocatalytic performance of material was evaluated by the photoredution of degradation of Amoxicillin (AMX) antibiotic under visible light. Results show that the obtained WO_3/Ag_3VO_4 photocatalyst can significantly enhance photocatalytic activity in comparison with the pure WO_3 and Ag_3VO_4. The enhanced photocatalytic activity of WO_3/Ag_3VO_4 was predominantly attributed to the synergistic effect which increased visible-light absorption and facilitated the efficient separation of photoinduced electrons and holes.

Introduction

Photocatalytic degradation of antibiotics pollutants has recently become novel technology for wastewater purification [1-3]. Numerous photocatalysts including TiO_2, ZnO, WO_3, $BiVO_4$, g-C_3N_4, $FeVO_4$, Ag_3VO_4, AgI and Ag_3PO_4 have been investigated for photocatalytic degradation of various organic pollutants [1-8]. However, the wide band gap energy (Eg ≥ 3,0 eV) and/or fast recombination rate of photo-excited electrons and holes are major disadvantages of these photocatalysts, leading to their low photocatalytic activity and/or the solar light could not be utilized as excitation source for photocatalysis. An efficient photocatalyst working well under visible light for degradation of organic pollutants (pesticides, antibiotic...) should have narrow band gap energy [9]. Recently, tungsten materials, in particularly WO_3, which are narrow band gap energy materials (2.8 eV), have been considered as ideal visible light-driven photocatalysts utilizing incident solar light for photocatalysis [4, 9]. However, the use of single WO_3 as photocatalyst for degradation of antibiotics pollutants has been limited because of the fast recombination of photo-excited electrons and holes. In addition, the photocatalyst could only utilize photo-

https://doi.org/10.51316/jca.2022.053

excited holes in the valence band to react with H_2O for production of $HO^{\bullet}$ (a strong oxidative radical degrading organic pollutants into harmless inorganic compounds such as CO_2 and H_2O). Therefore, various studies have been conducted to enhance photocatalytic activity of the WO_3 photocatalysts. Many previous studies have been reported that combination of WO_3 with another photocatalyst to establish a heterojunction system could enhance electron and hole separation efficiency as well as prevent the recombination of photo-excited electrons and holes leading to increase in its photocatalytic activity [4, 9, 10]. Due to its high stability and responsiveness to visible light, silver vanadate (Ag_3VO_4), another moderate band gap energy material that has attracted significant attention [11-13]. However, the photocatalytic activity of the g- Ag_3VO_4 still suffers from low conversion efficiencies due to the fast recombination of generated electrons and holes, which is usually considered as a major barrier in the single component semiconductor photocatalyst. It is still necessary to find appropriate compounds to further enhance the photocatalytic performance of Ag_3VO_4. The Ag_3VO_4 modified by using other semiconductors to establish a heterojunction or direct Z scheme system have exhibited novel photocatalytic activity even under visible light [11-15].

In this paper, we intend to the development of coupling Ag_3VO_4 with WO_3 as a high-performance visible light photocatalyst. The well aligned straddling band structures in hybrids can restrain the photoinduced charge recombination and enhance the transfer of electron-hole pairs. The degradation of AMX as a model pollutant under visible light to evaluate photocatalytic activity of WO_3/Ag_3VO_4.

Experimental

Photocatalyst synthesis

To synthesize WO_3 photocatalyst, sodium tungstate dihydrate ($Na_2WO_4.2H_2O$) was mixed with citric acid ($C_6H_8O_7$) (ratio 5:3) before dissolving in deionized water by stirring (~10 mins) to attain a clear solution, which was continuously added HCl solution (6M) to adjust pH to 1 to obtain a yellow solution. The solution was kept stirring for 30 mins before conducting hydrothermal process at 120 ^oC for 12 hours. The obtained product was washed by distilled water to achieve neutral pH. The cleaned product was continuously calcinated at 500 ^oC for 2 hours to achieve WO_3.

To synthesize Ag_3VO_4, 10 g $AgNO_3$ was dissolved in distilled water and stirred for 1 h at room temperature. Then, 5 M NaOH was wise-dropped to the solution to achieve pH 10 (solution A). Solution B containing 2.3 g NH_4VO_3 dissolving in distilled water was slowly mixed and stirred with the solution A for next 1 h before centrifugating to achieve participate. Distilled water was also used to wash the participate to reach neutral pH before drying at 60 ℃ for 24 h to obtain Ag_3VO_4.

To synthesize Ag_3VO_4/WO_3, WO_3 was firstly dispersed in distilled water and $AgNO_3$ solution was dropped to the WO_3 suspension before stirring for 1 h. Then, the solution of NaOH (5 M) was also used to adjust pH of the suspension to 10. The NH_4VO_3 solution was wise dropped into the adjusted pH suspension, which was continuously stirred for next 7 h in dark condition before centrifugating to achieve participate. Distilled water was also used to wash the obtained participate to reach neutral pH. The washed product was dried at 60 ℃ for 24 h to get Ag_3VO_4/WO_3 (WA).

Characterization methods

The prepared materials were carefully analyzed by an X-ray diffractometer (XRD, Bruker, AXS D8) to investigate their microstructure. UV–vis absorption spectra of these photocatalysts have been conducted on a UV – Visible spectrophotometer ((UV–Vis, Shimadzu, UV-3101PC)). Infrared spectroscopy was recorded on an 760 IR spectrometer (Nicolet-USA). Photoluminescence spectra (PL) were carried out on a Fluoromax-4-type spectrophotometer (Jobin–Yvon Co, France). Energy dispersive X-ray spectroscopy was determined on a S-4800 spectrophotometer (EDX, Hitachi – Japan).

Photocatalysis test

Photocatalysis experiments were carried out with an aqueous solution of amoxicillin solution (20 ppm) with a dosage of 0.5 g/L. The adsorption-desorption equilibrium was archived after 150 minute stirring without irradiation. After that, a LED lamp (220 V-30 W) was turned on to provide visible light. During irradiation time, every 30 min, 5 mL sample was taken out for filtration to determine remained amoxicillin. In detail, the filtrated solution was mixed with another solution containing benzoic acid, hydrochloric acid, sodium nitride and ammonium hydroxide for complexion. The obtained product was analyzed by an UV–vis absorption spectrometer at 435 nm.

https://doi.org/10.51316/jca.2022.053

Results and discussion

Materials characterization

The crystalline structures and phases of Ag_3VO_4, WO_3 and WO_3/Ag_3VO_4 photocatalysts were characterized by XRD. The XRD patterns of the obtained materials were shown in the Figure 1.

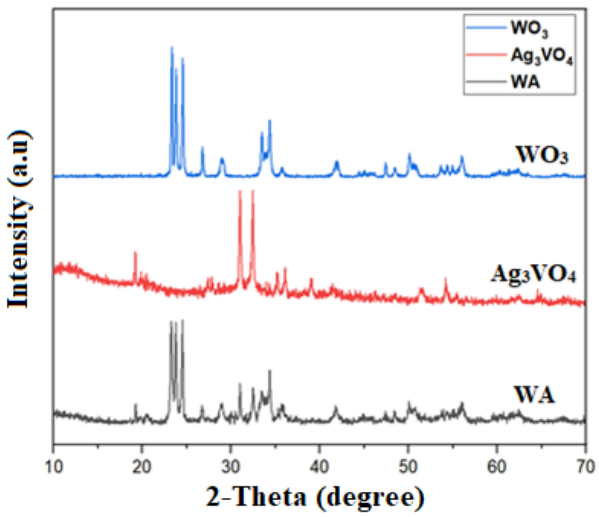

Figure 1: XRD patterns of WO_3, Ag_3VO_4 and WO_3/Ag_3VO_4

According to the XRD pattern of the WO_3 indicated that observed peaks at 2θ of 19.33◦, 30.98◦, 32.42◦, 35.21◦, 35.98◦ and 38.97◦ and 54.27◦ in the Ag3VO4 XRD pattern were indexed as (011), (−121), (121), (301), (202), (022) and (331) planes of the monoclinic typical Ag_3VO_4 sample (JCPDS No. 43-0542) [16, 17]. Major triplet peaks of pure WO_3 XRD pattern exhibited major triplet peaks at 2θ of 23.23◦, 23.72◦, and 24.41◦, which corresponded to (002), (020), and (200) planes of the typical monoclinic WO_3 sample (JCPDS No. 43-1035) [18]. For WO_3/Ag_3VO_4 material showed two sets of characteristic peaks attributing to the WO_3 and Ag_3VO_4 phases, suggesting that both components existed in the synthesized materials.

The optical properties of WO_3, Ag_3VO_4 and WO_3/Ag_3VO_4 were investigated by UV–Vis DRS. As shown in Figure 2, all samples exhibit strong absorption in the ultraviolet and part of the visible region (250–460 nm) and weak absorption in the visible region (460–800 nm). The optical absorption spectra also show that visible light absorption of the prepared WO_3/Ag_3VO_4 materials were better than that of single WO_3 and Ag_3VO_4 materials.

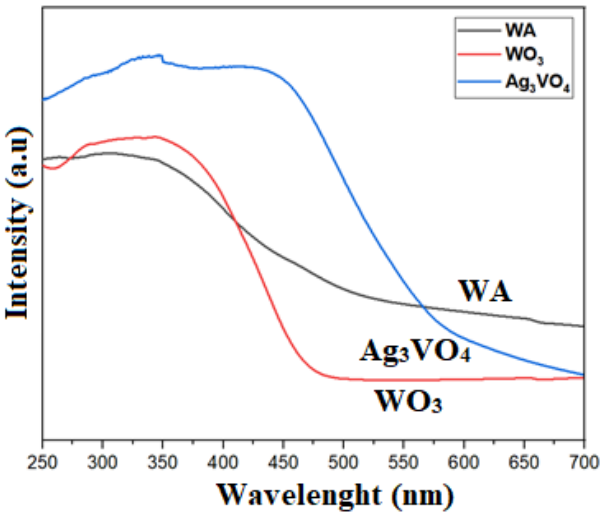

Figure 2: UV–Vis diffuse reflectance spectra of WO_3, Ag_3VO_4 and WO_3/Ag_3VO_4

The calculated band-gap energies of the WO_3, Ag_3VO_4 and WO_3/Ag_3VO_4 were 2.78, 2.21 and 2.74 eV, respectively (Fig. 3).

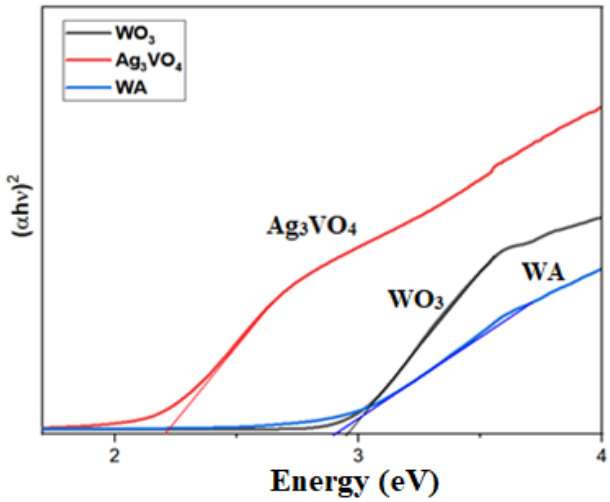

Figure 3: Tauc plots of WO_3, Ag_3VO_4 and WO_3/Ag_3VO_4

The PL emission spectra were employed to investigate the combination and separation of the photoinduced carriers, which played a crucial role in photocatalytic reactions. The WO_3, Ag_3VO_4 and WO_3/Ag_3VO_4 PL spectra were shown in Figure 4. Pure WO_3 and Ag_3VO_4 had strong PL peak intensity, the WO_3/Ag_3VO_4 heterojunction displayed lower intensity. The low PL emission intensity corresponds to the high photocatalytic performance due to the lower recombination efficiency of the photoinduced electron-hole pairs [4, 9]. Thus, the formation of heterojunction successfully solved the problem of easy recombination of photogenerated charges of single materials. The photocatalyst WO_3/Ag_3VO_4 shows a lowest luminescence emission among the prepared materials.

https://doi.org/10.51316/jca.2022.053

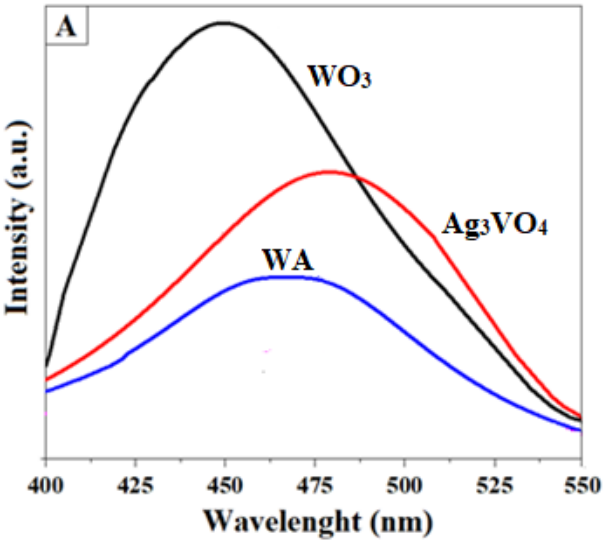

Figure 4: PL spectra of WO_3, Ag_3VO_4 and WO_3/Ag_3VO_4

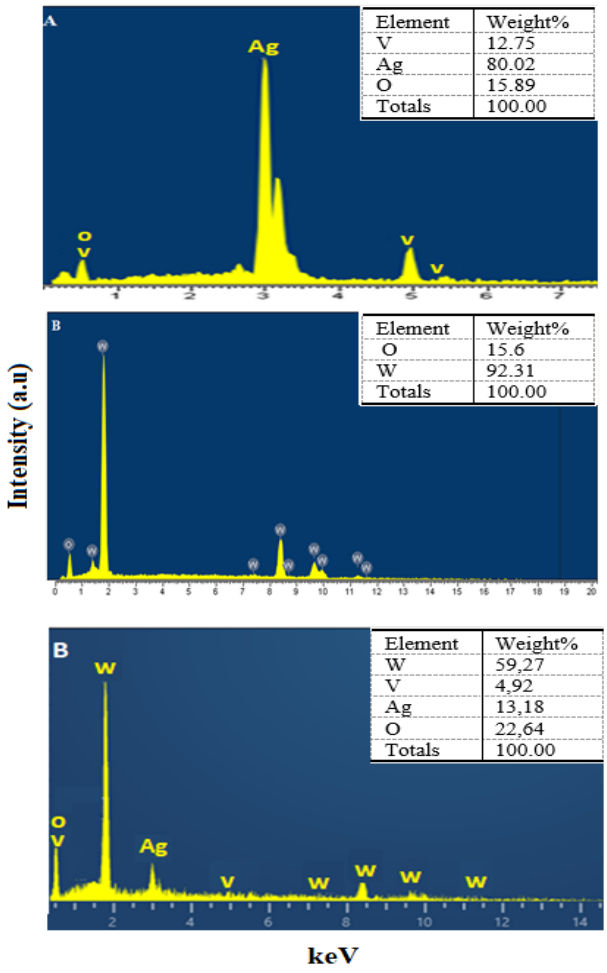

Figure 5: EDX spectra of Ag_3VO_4 (a), WO_3 (b) and WO_3/Ag_3VO_4 (c)

Elemental composition identified by EDX is compatible with the chemical structure of WO_3, Ag_3VO_4 and WO_3/Ag_3VO_4 materials. The WO_3, Ag_3VO_4 and WO_3/Ag_3VO_4 EDX spectra were shown in Figure 5.

The obtained EDX spectrum (Fig 5) showed that tungsten (observed peaks at 7,43, 8,45 and 9,64 keV), oxygen (0,51 keV), silver (3,1 keV), and vanadi (0,45 and 5,42 keV) were all detected. This indicated WO_3/Ag_3VO_4 was successfully synthesized.

The molecular structure of the synthesized WO_3, Ag_3VO_4 and WO_3/Ag_3VO_4 was studied using infrared spectroscopy with a spectrometer in the range 500–4000 cm^{-1}. The IR spectra of synthesized samples are shown in Figure 7. In the IR spectrum of Ag_3VO_4, the absorption peak at 745 and 868 cm^{-1} corresponds to Ag-V and V-O in VO_4^{3-} group [12]. For the WO_3 crystalline structure, the active mode vibrations of the W=O (870 cm^{-1}), W–O (686 cm^{-1}) bonds are owing to the octagonal structure [19]. In the binary component of WO_3/Ag_3VO_4, two the characteristic peaks of Ag_3VO_4 at 745 and 868 cm^{-1} were obscured after the introduction of WO_3 and vibrational modes at 830–852 cm^{-1} corresponding to the W–O–W bonds is WO_4 or WO_6. The peak at 912–938 cm−1 indicates the vibration of the W–O− and W=O bond of WO_4 and WO_6, indicating the coexistence of WO_3 and Ag_3VO_4 semiconductors.

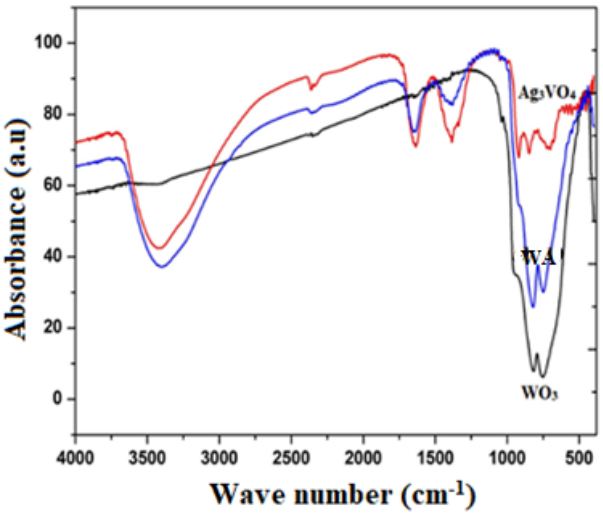

Figure 6: IR spectra of WO_3, Ag_3VO_4 and WO_3/Ag_3VO_4

Photocatalytic activities

The AMX removal using WO_3, Ag_3VO_4 and WO_3/Ag_3VO_4 materials were presented in the Figure 7. The change in AMX concentration during photocatalysis under visible light was followed up by absorbances collected from UV-visible spectrophotometer at 435 nm.

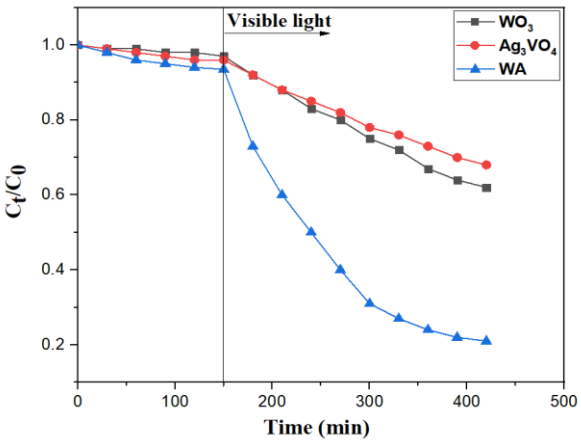

Figure 7: Conversion of AMX using WO_3, Ag_3VO_4 and WO_3/Ag_3VO_4

Figure 7 indicates that the photocatalytic activity of WO_3/Ag_3VO_4 was better than those of WO_3 and Ag_3VO_4. After 180 min irradiating by visible light, AMX degradation of the bare WO_3 and Ag_3VO_4 samples were 38.5 and 32.3%, respectively. When Ag_3VO_4 was hybridized with WO_3 to form Ag_3VO_4/WO_3 heterojunction, its photocatalytic amoxicillin degradation was remarkedly enhanced (79,86%) as compared to these pristine WO_3 and Ag_3VO_4 materials. Because of well hybridizing and matching band potentials between Ag_3VO_4 and WO_3, the photo-excited electrons at WO_3 conduction band would be transported from boundary to Ag_3VO_4 valence band and combined with its holes to inhibit charge recombination in each material resulting in accumulation of huge amounts of available electrons at Ag_3VO_4 conduction and holes in WO_3 valence (Fig. 8). The generated electrons and holes, which were high redox potentials, effectively participated in degradation of amoxicillin.

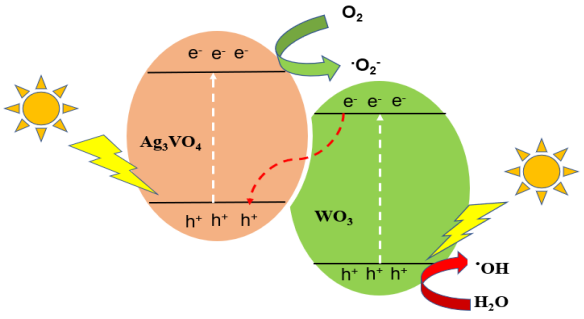

Figure 8: Amoxicillin degradation mechanism of the WO_3/Ag_3VO_4 photocatalyst.

Conclusion

WO_3/Ag_3VO_4 photocatalyst was synthesized and its characteristics were analyzed by XRD, SEM, IR and EDX. Photocatalyst particles were all in crystalline form. The estimated energy band gaps of the WO_3 and Ag_3VO_4 were 2.78 and 2.21 eV, respectively. Thus, both WO_3 and Ag_3VO_4 in WO_3/Ag_3VO_4 photocatalyst had suitable energy band gaps to absorb provided visible light for electrons jumping from VB to CB leaving holes at the VB. The WO_3/Ag_3VO_4 photocatalyst possess significantly improved visible light photocatalytic activity for AMX degradation compared with WO_3 and the Ag_3VO_4. The enhancement of photocatalytic efficiency under visible light is mainly attributed to the match of conduction and valence band levels between the WO_3 and Ag_3VO_4, which can induce the high separation of photo-generated electron–hole pairs in the heterojunction system.

Acknowledgments

This research is funded by Ministry of Education and Training of Vietnam under grant number B2021-DQN-08.

References

1. Y. Song, J. Gu, K. Xia, J. Yi, H. Chen, X. She, Z. Chen, C. Ding, H. Li, H. Xu, Applied Surface Science 467-468 (2019) 56-64. https://doi.org/10.1016/j.apsusc.2018.10.118
2. J. Zhang, Z. Ma, Materials Letters 216 (2018) 216–219. https://doi.org/10.1016/j.matlet.2018.01.035
3. Z. Wei, F. Liang, Y. Liu, W. Luo, J. Wang, W. Yao, Y. Zhu, Applied Catalysis B: Environmental 201 (2017) 600–606. https://doi.org/10.1016/j.apcatb.2016.09.003
4. Y. Yang, B. Liu, J. Xu, Q. Wang, X. Wang, G. Lv, J. Zhou, ACS Omega 7 (2022) 6035–6045. https://doi.org/10.1021/acsomega.1c06377
5. V. X Doorslaer, P. M. Heynderickx, K. Demeestere, K. Debevere, Van H. Langenhove, J. Dewulf, Applied Catalysis B: Environmental (2012) 150-156. https://doi.org/10.1016/j.apcatb.2011.09.029
6. R. Huo, X. L. Yang, Y. Q. Liu, Y. H. Xu, Materials research bulletin 88 (2017) 56-61. https://doi.org/10.1016/j.materresbull.2016.12.012
7. S. Yan, Z. Li, Z. Zou, Langmuir 25 (2009) 10397-10401. https://doi.org/10.1021/la900923z
8. Z. Yang, C. Deng, Y. Ding, H. Luo, J. Yin, Y. Jiang, P.

9. Zhang, Y. Jiang, Journal of Solid State Chemistry 268 (2018) 83-93. https://doi.org/10.1016/j.jssc.2018.07.031
10. M. Zhou, T. Tian, H. Zhonghua Wang, C. Ren, L. Zhou, Y-W Lin, L .Dou, ACS Omega 6 (2021) 26439–26453. https://doi.org/10.1021/acsomega.1c03694
11. Y. Wang, D. Chen, Y. Hu, L. Qin, J. Liang, X. Sun, Y. Huang, Sustainable Energy Fuels 4 (2020) 1681-1692. https://doi.org/10.1039/C9SE01158G
12. M. Tang, Y. Ao, C. Wang, P. Wang, Applied Catalysis B: Environmental 268 (2020) 118395. https://doi.org/10.1016/j.apcatb.2019.118395
13. K. Polat, M. Yurdakoc, Water Air Soil Pollution, 10 (2018) 229-331. https://doi.org/10.1007/s11270-018-3959-y
14. W. Zhao, Y. Feng, H. B. Huang, P. H. Zhou, J. Li, L. Zhang, B. L. Dai, J. M. Xu, F. X. Zhu, N. Sheng, D. Y. C. Leung, Applied Catalysis B: Environmental 245 (2019) 448-458. https://doi.org/10.1016/j.apcatb.2019.01.001
15. M. Yan, Y. Wu, F. Zhu, Y. Hua, W. Shi, Physical Chemistry Chemical Physics, 18 (2016) 3308-3315. https://doi.org/10.1039/C5CP05599G
16. T. Zhu, Y. Song, H. Ji, Y. Xu, Y. Song, J. Xia, H. Li, Chemical Engineering Journal 271 (2015) 96-105. https://doi.org/10.1016/j.cej.2015.02.018
17. Z. Liu, L. Chen, C. Piao, J. Tang, Y. Liu, Y. Lin, D. Fang, J. Wang, Applied Catalysis A: General 623 (2021) 118295. https://doi.org/10.1016/j.apcata.2021.118295
18. L. Jing, Y. Xu, C. Qin, J. Liu, S. Huang, M. He, H. Xu, H. Li, Materials research bulletin 95 (2017) 607–615. https://doi.org/10.1016/j.materresbull.2017.06.003
19. A. Dehdar, G. Asgari, M. Leili, T. Madrakian, A. Seid-mohammadi, Journal of Environment Management 297 (2021) 113338.
20. P.S. Kolhe, P.S. Shirke, N. Maiti, M.A. More, K.M. Sonawane, Journal of Inorganic and Organometallic Polymers and Materials 29 (2018) 41-48. https://doi.org/10.1007/s10904-018-0962-0